ChemComm

COMMUNICATION

View Article Online
View Journal | View Issue

Cite this: *Chem. Commun.*, 2024, **60**, 9408

Received 29th June 2024,
Accepted 2nd August 2024

DOI: 10.1039/d4cc03216k

rsc.li/chemcomm

Template-assisted synthesis of hollow anthraquinone-based covalent organic frameworks for aqueous zinc-ion hybrid supercapacitors†

Verónica Montes-García, [a] Cataldo Valentini, [bc] Denys Klymovych,[a] Wojciech Kukułka,[b] Linghao Shi,[a] Violetta Patroniak, [c] Paolo Samorì *[a] and Artur Ciesielski *[ab]

Anthraquinone-based hollow COFs were synthesized *via* a template-assisted method involving polystyrene nanospheres as the hard template, which enabled doubling the specific capacitance and energy density compared to non-templated COFs. Our approach can be extended to other COFs, offering a promising strategy for enhancing the performance of COF-based electrodes in energy storage applications.

Covalent organic frameworks (COFs) are a class of crystalline porous organic materials composed of light elements (such as H, B, C, N, and O) linked by covalent bonds.[1] By carefully selecting building blocks and optimizing synthesis conditions, COFs' structures and properties can be finely tuned to render them suitable for applications ranging from gas storage,[2] catalysis,[3] drug delivery[4] or sensing,[5] to energy storage.[6] In particular, COFs have garnered attention as electrode materials for supercapacitors and metal-ion batteries due to their high surface area, tunable porosity, and ability to undergo reversible redox reactions, which are crucial for enhancing energy storage capacity and cycling stability in these devices.[7] However, the targeted design of COFs with desired electrochemical properties continues to be a major focus in the fields of materials science and nanotechnology. Since the seminal paper by Yaghi and co-workers reporting the first COF in 2005,[1a] substantial efforts have been dedicated to advancing this field. The electrochemical performance of COFs is significantly influenced by their physicochemical properties, including surface area, porosity, as well as their ionic and electrical conductivity. These characteristics directly affect the ability of COFs to facilitate charge transfer and ion diffusion within their structures.[8] Furthermore, the topology of COFs plays a pivotal role in determining their physicochemical properties and hence their electrochemical behaviour, impacting parameters such as (electro)-chemical stability and accessibility of active sites. Nevertheless, predicting the topology of COFs remains a significant challenge during synthesis, hindering the precise tailoring of their properties for specific applications.[9] A promising strategy to overcome this limitation relies on the use of template-assisted methods.[10] Templated synthesis approaches have provided precise control over the design and synthesis of structurally well-defined zeolites,[11] MOFs[12] and COFs,[13] allowing for fine-tuning of properties and performance. Depending on the template's geometrical characteristics, these methods can be classified into three main types: hard template, soft template, and self-template methods.[10] The hard-template method is widely employed to create materials with hierarchical hollow or multi-pore-penetrating structures. COFs synthesized using hard templates retain their original micropores and develop additional mesopores or macropores that correspond to the voids left after removing the template. Hard templates include rigid porous solids with nanoscale or microscale characteristics, such as polymer nanoparticles, carbon materials, SiO_2 nanoparticles or polystyrene (PS) microspheres.[10] PS microspheres offer advantages as hard templates, including precise size control, dense packing, easy removal, and robust structural support during COF shell growth.[14] They facilitate the creation of hierarchically porous COFs (HP-COFs) with uniform mesopores or macropores.[15] Recently, HP-three dimensional-COFs (HP-3D-COFs) have been fabricated using PS microspheres as hard templates, demonstrating superior performance in proton conduction,[15] electrocatalysis[16] and ion sorption.[14] While PS microspheres have been used as a template for the fabrication of HP-3D-COFs, they have never been applied for the fabrication of hollow COFs (*i.e.*, microparticles with nanometer-thick shells). As demonstrated in the pioneering work of Kuo *et al.*, hollow COFs would offer significant advantages for energy storage applications.[17] Their thin shell structure maximizes exposed

[a] *Université de Strasbourg, CNRS, ISIS 8 allée Gaspard Monge, Strasbourg 67000, France. E-mail: samori@unistra.fr, ciesielski@unistra.fr*
[b] *Centre for Advanced Technologies, Adam Mickiewicz University, Uniwersytetu Poznańskiego 10, Poznań 61-614, Poland*
[c] *Faculty of Chemistry, Adam Mickiewicz University, Uniwersytetu Poznańskiego 8, Poznań 61-614, Poland*

† Electronic supplementary information (ESI) available. See DOI: https://doi.org/10.1039/d4cc03216k

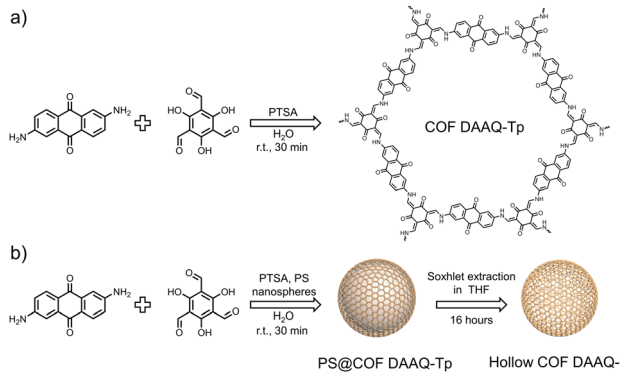

Fig. 1 Synthesis pathways for (a) COF-DAAQ-Tp and (b) hollow COF-DAAQ-Tp.

surface area, providing more active sites for electrochemical reactions and facilitating efficient charge storage and transfer. Additionally, thin shells reduce ion diffusion path lengths, allowing faster ion transport and shorter charge–discharge times, crucial for high-power density applications. To the best of our knowledge, no other studies have explored hollow COFs for energy storage applications.

In this study, we synthesize hollow COFs using an anthraquinone-based COF through a template-assisted method involving PS nanospheres and assess their performance in energy storage applications. We compare the physicochemical properties and electrochemical performance of the hollow COF with those of the analogous COF synthesized in the absence of PS nanospheres. The COF synthesis involves a condensation reaction between the organic monomers 1,3,5-triformylphloroglucinol (Tp) and 2,6-diaminoanthraquinone (DAAQ), catalyzed by *p*-toluenesulfonic acid (PTSA), resulting in COF-DAAQ-Tp (Fig. 1a).

For the hollow COF synthesis, an analogous reaction is performed in the presence of PS nanospheres with a diameter of 300 nm, which act as a template for controlled COF growth on their surface (PS@COF-DAAQ-Tp). Subsequently, the PS nanospheres are removed *via* Soxhlet extraction with tetrahydrofuran (THF), yielding the hollow COF DAAQ-Tp (Fig. 1b). In imine-linked COFs, when hydroxyl groups are located next to the aldehyde moieties within one of the building units, tautomerization from the enol-imine to the keto-enamine form typically takes place. Fourier-transform infrared (FTIR) spectra (Fig. S1, ESI†) of COF-DAAQ-Tp (black curve) and hollow COF-DAAQ-Tp (red curve) provide initial evidence of successful COF syntheses and the coexistence, in both cases, of imine and β-ketoenamine forms.[18] Both COFs exhibit the absence of the primary amine stretching vibration (3300–3500 cm^{-1}) of the building unit, indicating that all the monomers have fully reacted in the synthesis process. The presence of the C═N stretching vibration (1680 cm^{-1}) confirms the imine form, while the shift of the C═O stretching vibration signal to 1615 cm^{-1} compared to the building unit (C═O around 1658 cm^{-1})[18] and the presence of C–N stretching vibration (1250 cm^{-1}) are indicative of β-ketoenamines.

X-ray photoelectron spectroscopy (XPS) analysis is then performed (Fig. 2a and b and Fig. S2–S4, ESI†) to gain deeper

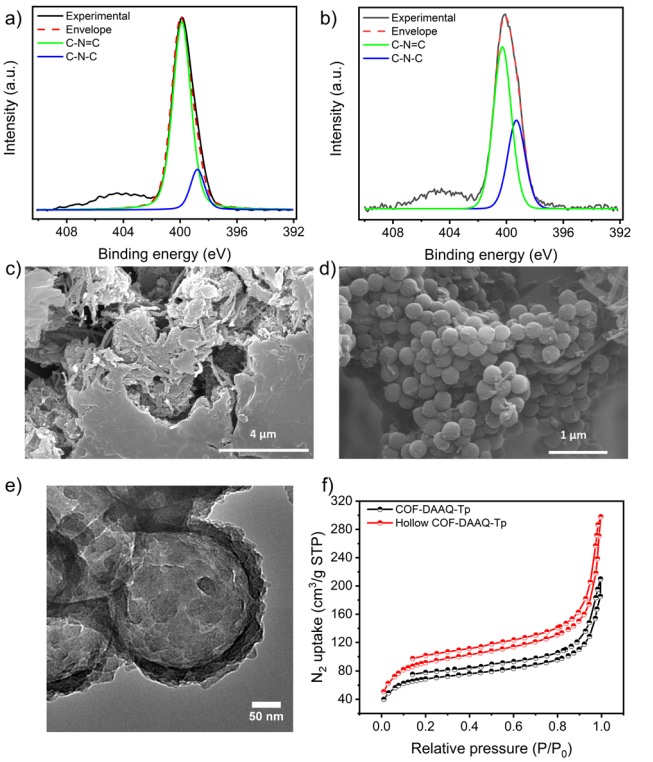

Fig. 2 (a) and (b) N 1s XPS analysis of (a) COF-DAAQ-Tp, and (b) hollow COF-DAAQ-Tp, (c) and (d) SEM images of (c) PS@COF-DAAQ-Tp and (d) COF-DAAQ-Tp, (e) HRTEM image of hollow COF-DAAQ-Tp and (f) BET surface area of COF-DAAQ-Tp (black curve) and hollow COF-DAAQ-Tp (red curve).

insight into the chemical composition of the as-prepared COFs. The high-resolution N 1s spectra of COF-DAAQ-Tp (Fig. 2a) and hollow COF-DAAQ-Tp (Fig. 2b) display two main peaks at 398.7 and 400 eV, which correspond to C–N (from β-ketoenamine form) and C═N (from imine form) bonds, respectively. Interestingly, the content of the β-ketoenamine form is higher in the hollow COF-DAAQ-Tp. Similarly, the high-resolution O 1s spectra of COF-DAAQ-Tp (Fig. S4, ESI,† bottom panel) and hollow COF-DAAQ-Tp (Fig. S4, ESI,† top panel) exhibit two peaks at 530.9 and 532.8 eV which correspond to C═O (from β-ketoenamine form) and C–O (from imine form) bonds, respectively, confirming the presence of both tautomeric forms in each COF.

Powder X-ray diffraction (PXRD) is employed to analyse the crystallinity of the COFs (Fig. S5, ESI†). Both COFs exhibit a sharp peak at 3.5°, as well as a broad peak with a maximum at 26.7°, corresponding to the reflection planes of 100, and 001 respectively, in full agreement with the simulated pattern reported in the literature (Fig. S5, ESI†).[18] The PXRD analysis confirms that using a template-supported synthesis does not affect the crystalline structure of the resulting COF. Thermogravimetric analyses (TGA) (Fig. S6, ESI†) show that both COFs exhibit good thermal stability with Td_{10} (temperature of thermal decomposition at 10% weight) of 295 °C and 375 °C for COF-DAAQ-Tp and hollow COF-DAAQ-Tp, respectively. The higher thermal stability of hollow COF-DAAQ-Tp could be related to the higher presence of β-ketoenamine form in its structure.

Scanning (transmission) electron microscopy (S(T)EM) and high- resolution TEM (HRTEM) are used to investigate the morphology of COFs and the shell thickness of the hollow COF-DAAQ-Tp. While the SEM image of COF-DAAQ-Tp (Fig. 2c) shows the absence of any regular morphology, the SEM image of PS@COF-DAAQ-Tp (Fig. 2d) exhibits a sphere-like shape with a shell thickness of 9.40 ± 1.15 nm (Fig. S8, ESI†). Importantly, the HR-TEM images (Fig. 2e and Fig. S7b, ESI†) and STEM image (Fig. S7a, ESI†) of hollow COF-DAAQ-Tp, provide compelling evidence of the formation of a spherical hollow COF or COF shell structure, with the PS nanospheres completely etched. This observation underscores the efficacy of using PS nanospheres as a hard templating agent in guiding the morphology of the COF material.

To investigate the porosity of COF-DAAQ-Tp and hollow COF-DAAQ-Tp, nitrogen adsorption–desorption isotherms at 77 K (Fig. 2f) are acquired. These isotherms could be classified as Type IV sorption and the calculated Brunauer–Emmett–Teller (BET) surface areas amount to 257 and 344 $m^2 g^{-1}$ for COF-DAAQ-Tp and hollow COF-DAAQ-Tp, respectively. Additionally, the Barrett–Joyner–Haleda (BJH) model is used to calculate the pore distribution (Fig. S9, ESI†), showing a microporous nature with average pore sizes of 1.1 and 2.2 nm for COF-DAAQ-Tp and hollow COF-DAAQ-Tp, respectively. Overall, BET analysis unequivocally proves that the hollow COF demonstrates a larger surface area and higher average pore size compared to its non-templated counterpart.

The electrochemical performance of COF-DAAQ-Tp and hollow COF-DAAQ-Tp is assessed by employing them as cathode materials in zinc-ion hybrid supercapacitors (Zn-HSCs). Zn-HSCs have garnered significant interest as potential successors to current energy storage devices, lithium-ion batteries (LIBs), primarily due to their inherent safety features, cost-effectiveness, high specific capacity (820 mA h g^{-1}), and the relatively low redox potential (−0.76 V *vs.* standard hydrogen electrode) of Zn anodes. A two-electrode configuration that consists of a COF-based cathode, Zn foil as anode and 4 M aqueous solution of zinc trifluoromethanesulfonate ($Zn(CF_3SO_3)_2$) as electrolyte is employed. The cyclic voltammetry (CV) curves of COF-DAAQ-Tp (Fig. 3a) and hollow COF-DAAQ-Tp (Fig. 3b) COF at various scan rates (from 0.01 to 1 V s^{-1}) in a potential window from 0 to 1.8 V show two clear peaks that correspond to the insertion/extraction processes of Zn^{2+} ions. In order to gain insights into the charge storage mechanism of the COF-based electrodes, the kinetics of the electrochemical processes occurring at both electrode materials are analysed using the procedure proposed by Wu *et al.*[19] The peak current (i) correlates to the scan rate (ν) according to the eqn (4) (see ESI†). The values of b parameter define the dominating kinetics of the electrochemical process, where 0.5 corresponds to the diffusion-limited electrochemical process and 1 indicates a capacitive-limited process. The average b-values for COF-DAAQ-Tp and hollow COF-DAAQ-Tp (Fig. S10a–d, ESI†) amount to 0.81 and 0.85, respectively, indicating a hybrid storage mechanism for both COF-based electrodes, predominantly ruled by a capacitive contribution and partial diffusion-controlled contribution. To further analyse the capacitive contribution and the diffusion-controlled contribution at a specific scan rate, eqn (4)

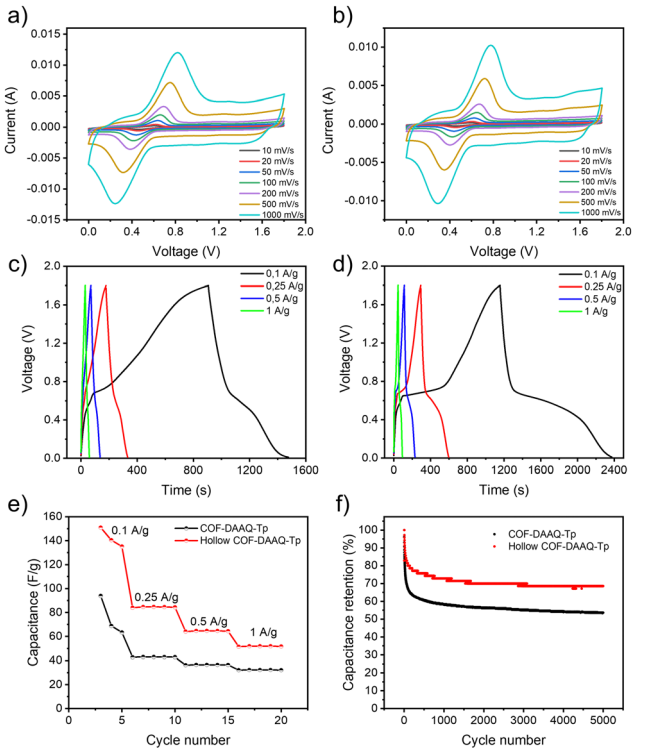

Fig. 3 Electrochemical characterization of COF-DAAQ-Tp and hollow COF-DAAQ-Tp. (a) and (b) CV curves at different scan rates (0.01–1 V s^{-1}), and (c) and (d) GCD at different current densities (0.1–1 A g^{-1}) for (a) and (c) COF-DAAQ-Tp and (b) and (d) hollow COF-DAAQ-Tp, (e) rate performance COF-DAAQ-Tp (black curve) and hollow COF-DAAQ-Tp (red curve) at different current densities (0.1–1 A g^{-1}), and (f) cycling performance at current density 1 A g^{-1} for 5000 charge/discharge cycles of COF-DAAQ-Tp (black curve) and hollow COF-DAAQ-Tp (red curve).

can be divided into two parts, as shown in eqn (5) (see ESI†) The capacitive and diffusion-controlled contribution values at different rates are calculated and shown in Fig. S10e and S11 (ESI†) for COF-DAAQ-Tp and Fig. S10f and S12 (ESI†) for hollow COF-DAAQ-Tp. At a scan rate of 0.01 V s^{-1}, the capacitive contributions are 27.2% and 34.6% for COF-DAAQ-Tp and hollow COF-DAAQ-Tp, respectively. With the increase in scan rate, the capacitive contribution rises and at a scan rate of 1 V s^{-1} it represents 78.9% and 84.1% of the total contribution for COF-DAAQ-Tp and hollow COF-DAAQ-Tp, respectively. The higher capacitive contribution observed in the hollow COF-DAAQ-Tp, in contrast to the COF-DAAQ-Tp, may be attributed to the improved accessibility of active groups facilitated by the larger active surface area of the hollow COF-DAAQ-Tp.

Electrochemical impedance spectroscopy (EIS) is analyzed using Nyquist plots (Fig. S13, ESI†). R_{ct} (charge transfer resistance) represents the resistance of electrochemical reactions at the electrode surface. Their values for COF-DAAQ-Tp and hollow COF-DAAQ-Tp amount to 741 and 380 Ω, respectively. The lower R_{ct} of the hollow COF-DAAQ-Tp in comparison to the COF-DAAQ-Tp indicates a higher ionic conductivity for hollow COF-DAAQ-Tp as a result of its higher porosity.

Fig. 3c and d display the galvanostatic charge/discharge (GCD) profiles of COF-DAAQ-Tp (Fig. 3c) and hollow COF-DAAQ-Tp

(Fig. 3d) in a potential window from 0 to 1.8 V at the current densities between 0.1 and 1 A g^{-1}. The GCD profiles exhibit plateaus for both COFs, which confirms the hybrid nature of the electrode materials. The electrochemical performance is expressed by means of gravimetric capacitance, which was calculated from the GCD profiles (see ESI†).

As a result of its larger active surface area, and higher porosity, the hollow COF-DAAQ-Tp exhibits nearly twice gravimetric capacitance compared to the COF-DAAQ-Tp (142.1 *versus* 75.4 F g^{-1} at a current density of 0.1 A g^{-1}), (Fig. 3e). Similarly, the energy density of the hollow COF-DAAQ-Tp is twice that of the COF-DAAQ-Tp (17.8 *versus* 8.67 W h kg^{-1}), while power density remains similar (697.6 W kg^{-1} for COF-DAAQ-Tp and 603.9 W kg^{-1} for hollow COF-DAAQ-Tp). While hollow COF-DAAQ-Tp may not demonstrate the highest performance compared to other state-of-the-art cathode materials for Zn-HSCs (refer to Table S1, ESI†), our results emphasize that the template-assisted synthesis method significantly enhances both the electrochemical performance and the predictability of the morphological characteristics of COF materials. The long-term stability of the prepared COF-based electrodes was investigated using GCD at a current density of 1 A g^{-1} for 5000 charge/discharge cycles. Although the capacitance of COF-DAAQ-Tp decreases to approximately 66% after the first 50 charge/discharge cycles, the hollow COF exhibits significantly better long-term stability (capacitance retention above 70% after 5000 charge/discharge cycles) (Fig. 3f). This rapid initial decay might be associated with the formation of a solid electrolyte interphase (SEI) layer, which may form on the surface of the zinc anode.[20] This enhanced stability is attributed to its higher chemical stability, as evidenced by XPS analysis, which shows a greater presence of the β-ketoenamine form in the hollow COF-DAAQ-Tp compared to the COF-DAAQ-Tp.

In summary, we successfully synthesized hollow COF shells using a template-assisted method involving PS nanospheres and an anthraquinone-based COF and evaluated their energy storage performance. The hollow COF-DAAQ-Tp exhibited a predictable spherical morphology, a larger active surface area (344 m^2 g^{-1}), and a higher average pore size (2.2 nm) compared to its non-templated counterpart (257 m^2 g^{-1}, 1.1 nm, respectively). This increased porosity improved access to the COF's carbonyl redox active sites, resulting in significantly higher electrochemical performance. Specifically, the templated COF achieved nearly double the specific capacitance (142.1 F g^{-1} *vs.* 75.4 F g^{-1}), energy density (17.8 W h kg^{-1} *vs.* 8.67 W h kg^{-1}), and a higher capacitive contribution (84.1% *vs.* 78.9% at 1 V s^{-1}). Additionally, the hollow COF-DAAQ-Tp showed better long-term stability with capacitance retention above 70% after 5000 cycles, attributed to its higher chemical stability indicated by a greater presence of the β-ketoenamine form. Overall, this approach can be extended to other COFs whose building monomers are soluble in acid media (*e.g.*, melamine, 2,5-dihydroxyterephthalaldehyde and heptaazaphenalene, to name a few) to optimize their properties, making them more suitable as electrode materials for energy storage applications.

This work was supported by the National Science Centre (grant no. 2022/47/B/ST4/02310 and 2020/36/C/ST5/00247). We also acknowledge support from the Interdisciplinary Thematic Institute SysChem *via* the IdEx Unistra (ANR-10-IDEX-0002) within the program Investissement d'Avenir program, the Foundation Jean-Marie Lehn and the Institut Universitaire de France (IUF).

Data availability

Data available on request from the authors. The data that support the findings of this study are available from the corresponding author, [Artur Ciesielski], upon reasonable request.

Conflicts of interest

There are no conflicts to declare.

Notes and references

1 (*a*) A. P. Côté, A. I. Benin, N. W. Ockwig, M. O'Keeffe, A. J. Matzger and O. M. Yaghi, *Science*, 2005, **310**, 1166; (*b*) Y. Su, B. Li, H. Xu, C. Lu, S. Wang, B. Chen, Z. Wang, W. Wang, K.-I. Otake, S. Kitagawa, L. Huang and C. Gu, *J. Am. Chem. Soc.*, 2022, **144**, 18218.
2 H. Furukawa and O. M. Yaghi, *J. Am. Chem. Soc.*, 2009, **131**, 8875.
3 (*a*) Y. Su, B. Li, Z. Wang, A. Legrand, T. Aoyama, S. Fu, Y. Wu, K.-I. Otake, M. Bonn, H. I. Wang, Q. Liao, K. Urayama, S. Kitagawa, L. Huang, S. Furukawa and C. Gu, *J. Am. Chem. Soc.*, 2024, **146**, 15479; (*b*) S. Wang, Z. Xie, D. Zhu, S. Fu, Y. Wu, H. Yu, C. Lu, P. Zhou, M. Bonn, H. I. Wang, Q. Liao, H. Xu, X. Chen and C. Gu, *Nat. Commun.*, 2023, **14**, 6891.
4 Q. Fang, J. Wang, S. Gu, R. B. Kaspar, Z. Zhuang, J. Zheng, H. Guo, S. Qiu and Y. Yan, *J. Am. Chem. Soc.*, 2015, **137**, 8352.
5 X. Liu, D. Huang, C. Lai, G. Zeng, L. Qin, H. Wang, H. Yi, B. Li, S. Liu, M. Zhang, R. Deng, Y. Fu, L. Li, W. Xue and S. Chen, *Chem. Soc. Rev.*, 2019, **48**, 5266.
6 S. Kandambeth, V. S. Kale, O. Shekhah, H. N. Alshareef and M. Eddaoudi, *Adv. Energy Mater.*, 2022, **12**, 2100177.
7 X. Zhao, P. Pachfule and A. Thomas, *Chem. Soc. Rev.*, 2021, **50**, 6871.
8 M. Sajjad and W. Lu, *J. Energy Storage*, 2021, **39**, 102618.
9 (*a*) J. Hu, J. Zhang, Z. Lin, L. Xie, S. Liao and X. Chen, *Chem. Mater.*, 2022, **34**, 5249; (*b*) L. Huang, J. Yang, Y. Asakura, Q. Shuai and Y. Yamauchi, *ACS Nano*, 2023, **17**, 8918.
10 X. Wang, Z. Mu, P. Shao and X. Feng, *Chem. – Eur. J.*, 2024, **30**, e202303601.
11 K. Zhang, Z. Liu, X. Yan, X. Hao, M. Wang, C. Li and H. Xi, *Langmuir*, 2017, **33**, 14396.
12 J. Yang, K. Li and J. Gu, *ACS Mater. Lett.*, 2022, **4**, 385.
13 Z. Xiong, B. Sun, H. Zou, R. Wang, Q. Fang, Z. Zhang and S. Qiu, *J. Am. Chem. Soc.*, 2022, **144**, 6583.
14 T. Liu, Y. Zhao, M. Song, X. Pang, X. Shi, J. Jia, L. Chi and G. Lu, *J. Am. Chem. Soc.*, 2023, **145**, 2544.
15 W. Zou, G. Jiang, W. Zhang, L. Zhang, Z. Cui, H. Song, Z. Liang and L. Du, *Adv. Funct. Mater.*, 2023, **33**, 2213642.
16 X. Zhao, P. Pachfule, S. Li, T. Langenhahn, M. Ye, C. Schlesiger, S. Praetz, J. Schmidt and A. Thomas, *J. Am. Chem. Soc.*, 2019, **141**, 6623.
17 A. F. M. El-Mahdy, C. Young, J. Kim, J. You, Y. Yamauchi and S.-W. Kuo, *ACS Appl. Mater. Interfaces*, 2019, **11**, 9343.
18 C. R. DeBlase, K. E. Silberstein, T.-T. Truong, H. D. Abruña and W. R. Dichtel, *J. Am. Chem. Soc.*, 2013, **135**, 16821.
19 X. Wu, J. J. Hong, W. Shin, L. Ma, T. Liu, X. Bi, Y. Yuan, Y. Qi, T. W. Surta, W. Huang, J. Neuefeind, T. Wu, P. A. Greaney, J. Lu and X. Ji, *Nat. Energy*, 2019, **4**, 123.
20 Y. Li, Z. Yu, J. Huang, Y. Wang and Y. Xia, *Angew. Chem., Int. Ed.*, 2023, **62**, e202309957.